TISSUE ENGINEERING: Part A
Volume 19, Numbers 3 and 4, 2013
© Mary Ann Liebert, Inc.
DOI: 10.1089/ten.tea.2012.0135

Design and Validation of a Bioreactor for Simulating the Cardiac Niche: A System Incorporating Cyclic Stretch, Electrical Stimulation, and Constant Perfusion

Liang Lu, BS, BME,[1] Matthias Mende, MD,[1] Xuegeng Yang, PhD,[2] Heinz-Felix Körber, Dipl Ing,[3] Hans-Joachim Schnittler, PhD,[4,*] Sönke Weinert, MSc,[5] Jürgen Heubach, PhD,[1] Carsten Werner, PhD,[6] and Ursula Ravens, MD, PhD[1]

To simulate the cardiac niche, a bioreactor system was designed and constructed to incorporate cyclic stretch, rhythmic electrical stimulation, and constant perfusion. The homogeneity of surface strain distribution across the cell culture substrate was confirmed with ARAMIS deformation analysis. The proliferation marker, Ki-67, detected in human umbilical vein endothelial cells and 3-[4,5-dimethyl-thiazol-2-yl]-2,5-diphenyltetrazolium bromide cytotoxicity assay performed on human atrial fibroblasts confirmed biocompatibility of this novel device. Cyclic stretch treatment for 24 h resulted in the perpendicular alignment of human atrial fibroblasts. An electrical stimulation system containing carbon electrodes was characterized by electrochemical impedance spectroscopy and charge injection/recovery studies, which indicated that increased corrosive reactions were associated with a higher input voltage and prolonged pulse duration. Field stimulation delivered through this system could induce rhythmic contractions in adult rat ventricular myocytes, with contractile characteristics similar to those paced in a standard field stimulation chamber. In conclusion, this bioreactor provides a novel tool to study the interaction between physical stimulation and cardiac cell physiology.

Introduction

Cells residing in the cardiac niche are constantly experiencing physical stimuli, including cyclic mechanical stretch and electrical pulses. These physical signals are known to influence a variety of cellular functions. For instance, cyclic stretch has been shown to mediate growth factor secretion[1] and calcium-handling properties[2] in cardiomyocytes and alter the production of extracellular matrix proteins in cardiac fibroblasts.[3,4] Isolated adult rat ventricular myocytes in primary culture subjected to continual electric field stimulation exhibit enhanced contractile properties and calcium-transient characteristics compared to non-stimulated quiescent cells.[5,6] All these studies underscore the influential role of physical stimulation in cultured cell monolayers or isolated single cells.

Furthermore, in cardiac tissue engineering studies, several biomimetic strategies have been developed to cultivate 3D tissue constructs in culture conditions that recapitulate one or more aspects of the native myocardial environment, including cyclic stretch,[7] electrical pulses,[8] "electro-tensile" stimulation,[9] constant fluid perfusion,[10–12] oxygenation via carriers through channeled scaffold,[12] and more recently, concerted medium perfusion and electrical stimulation,[13] all of which provide additional evidence on the functional improvement of 3D cardiac tissue constructs due to the application of physical stimuli.

In an effort to develop a novel tool to better understand how physical stimuli affect cell physiology, we designed and validated a bioreactor that incorporates cyclic stretch, electrical stimulation, and constant perfusion into one system. We introduce a list of engineering specifications that we

Part of these results have been published in an abstract form. Lu, L., Mende, M., Körber, H., Werner, C., and Ravens, U. Design and validation of a cyclic stretch bioreactor system for simulating the cardiac environment. Abstract #552. 75th Anniversary of Albert Szent-Györgyi's Nobel Prize Award. 25-3-2012.

[1]Department of Pharmacology and Toxicology, Medical Faculty "Carl Gustav Carus", Dresden University of Technology, Dresden, Germany.
[2]Institute of Fluid Mechanics, Chair of Magnetofluiddynamics, Measuring and Automation Technology, Technische Universität Dresden, Dresden, Germany.
[3]FORTECH UG, Dresden, Germany.
[4]Department of Physiology, Medical Faculty, Dresden University of Technology, Dresden, Germany.
[5]Internal Medicine/Cardiology, Angiology and Pneumology, Magdeburg University, Magdeburg, Germany.
[6]Max Bergmann Centre for Biomaterials, Leibniz Institute for Polymer Research Dresden, Dresden, Germany.
*Current affiliation: Institute of Anatomy, Münster, Germany.

envisage for an ideal system, and then provide a description on the design of the bioreactor, followed by surface strain analyses and characterization of the electrical stimulation system on the current prototype. The biocompatibility and the proper transduction of physical stimuli into biological responses are validated using human umbilical vein endothelial cells (HUVEC), human atrial fibroblasts, and adult rat ventricular myocytes.

Bioreactor Construction

Engineering specifications

The bioreactor was designed to apply both uniaxial cyclic stretch and electrical stimulation to cultured cells with a fluid inlet and outlet to allow constant perfusion. The design and development of the prototype were based on the following engineering specifications: (i) For simulating cardiac contraction, precisely controlled strain (of user-specified magnitude and frequency) should be applied homogeneously across the entire surface of cell culture substrate. (ii) Physiologically, electrical excitation triggers contractile activity; therefore, rhythmic electrical stimulation of various amplitude, frequency, and duration should be delivered via electrodes with a high charge-injecting capability and high resistance to irreversible electrochemical reactions. (iii) For optimal oxygen and nutrients supply, the bioreactor should have the inlet and outlet to allow constant flow of the cell culture medium. (iv) Materials used to build the bioreactor should be biocompatible and easy to sterilize by autoclave. In case of stretching a monolayer of cultured cells, the stretchable substrate upon which the cells are seeded should allow surface modification and protein coating to facilitate cell attachment. (v) The device should be easy to handle, that is, robust and convenient for routine use in standard cell culture conditions.

Description of current prototype

The entire bioreactor system consists of a chamber, a driving system with a stepper motor and its control box, and an electrical stimulation system with carbon rod electrodes.

Design of the bioreactor chamber. A general schematic of the bioreactor chamber is shown in Figure 1. The casing of the chamber and most of auxiliary parts are made from polyether ether ketone polymer due to its superior mechanical strength and high resistance to chemical and thermal degradation. Uniaxial stretch is based on motor/cam/shaft mechanism: the edges of cell-seeded polymer substrates (blue) are clamped to two plastic brackets (Fig. 1A #2, 1 cm apart at rest). One bracket is pivoted to the stationary shaft (Fig. 1A #3), which attaches firmly to the wall of the bioreactor chamber, and the other bracket is pivoted to the driving shaft (Fig. 1A #4, B #10), which extends outside of the chamber. The orifice through which the driving shaft exits the chamber serves as ventilation opening to allow gas exchange. The end of the driving shaft is capped by a plastic cantilever (Fig. 1B #9), which has a metal pin as the rotating follower (Fig. 1B #8) pressed to the cam (eccentric disk, Fig. 1B #7) of the driving system. When in operation, the protrusion of the rotating cam tilts the cantilever and twists the shaft, thereby stretching the cell-seeded polymer substrate inside the chamber (Supplementary Movies M1 and M2; Supplementary Data are available online at www.liebertpub.com/tea).

The opposite ends of the bioreactor have two orifices (4 mm diameter, Figs. 1A #1 and 6B #6 and #8) to allow constant fluid flow through the chamber via rubber tubing. The top and bottom of the bioreactor chamber piece could be covered with glass slides ($76 \times 26 \times 1$ mm) to allow visual inspection during experiments (Supplementary Movies M2–M4).

Polydimethylsiloxane polymer substrate. Polydimethylsiloxane (PDMS) is selected as the stretchable substrate material due to its ease of molding, low cytotoxicity, oxygen permeability, and transparency. Briefly, a premixed solution of silicone (Sylgard 184, base:curing agent ratio = 10:1; Dow Corning) was poured into a custom-made polycarbonate casting mold (Fig. 2E) in a clean room environment, and the mold was left undisturbed for 72 h at room temperature to allow curing. The resulting PDMS substrates ($2\,\text{cm} \times 1\,\text{cm} \times 50\,\mu\text{m}$, Fig. 2B, left) were subsequently transferred and stored on a 10-cm cell culture dish (Nunclon, Cat #150350). To prevent dust contamination, the dish was sealed with parafilm and stored in an air-tight box until use. Note that the breadth side of the substrate has an arc-shaped indentation with a reinforced edge (Fig. 2B, arrow heads). When the PDMS substrate is stretched, the indented reinforced edges are straightened to provide an outward lateral strain to counter necking due to the Poisson effect. Such a design is intended to achieve a homogeneous strain distribution across the PDMS substrate.

FIG. 2. ARAMIS analysis of surface deformation. **(A)** The ARAMIS system assigns a set of color codes (bottom) to represent measured surface deformation. As shown, stretch (with 5% increments up to 30%) can be applied homogeneously and precisely across the entire membrane surface. An internal negative control and a tester for ARAMIS system's resolution, a drop of super glue was placed at the left-center of the membrane, so that the rigidity of dried glue minimizes deformation, which appears as a blue island of low strain. Surface strain maps represent the entire surface of PDMS substrate. **(B)** PDMS substrate. Left, intact PDMS substrate is transparent. Center, to enhance surface contrast for ARAMIS analysis, a PDMS substrate sample is coated with medical charcoal. White arrow heads indicate the indented, arc-shaped breadth edge (thickness = 1 mm). Thickness of length edges = 2 mm. Right, a 2 euro-cent coin (same size as a US penny) for size comparison. Scale in centimeters. **(C)** Screen shot from ARAMIS measurement. Overlaid images of PDMS substrate (black-white) and measured surface strain (green) to show the color code analysis spans the entire surface of the PDMS, with the exception of edges. Notice when the substrate is stretched, the breadth edges are straightened to provide an outward lateral strain. **(D)** Lateral strain color map at 30% applied stretch. Although lateral strain could be detected at the breadth edges, the majority of the PDMS substrate surface showed a green color, corresponding to 0% lateral strain. **(E)** Custom-made polycarbonate casting mold. Premixed PDMS was first poured into the mold, and the mold was closed (pink = hinge) and locked with screws (blue arrows). The mold was left at room temperature for 72 h to allow curing. White scale bar at bottom: 5 cm.

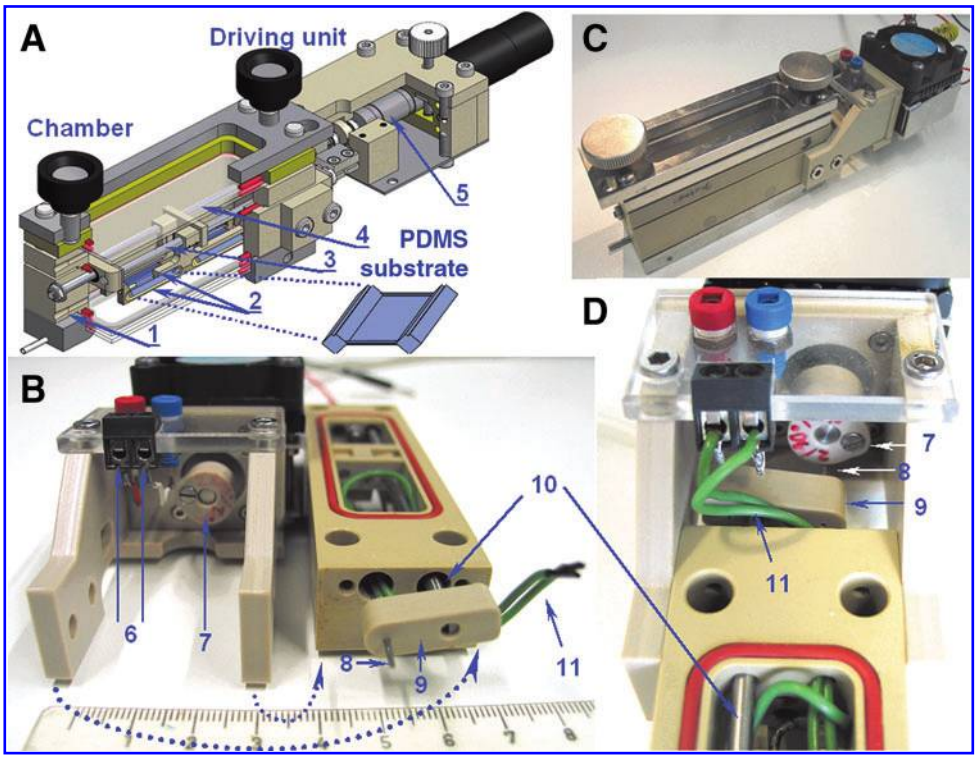

FIG. 1. Overview of the bioreactor. **(A)** A schematic representation of the conceptual design, front right view. (1) medium outlet, (2) plastic bracket, (3) stationary shaft, (4) driving shaft (corresponding to #10 in Fig. 1B), (5) stepper motor. Color code for materials: ivory = polyether ether ketone (PEEK), metallic gray = stainless steel, red = silicone rubber, blue = polydimethylsiloxane (PDMS) scaffold. **(B)** Photograph of core components of mechanical and electrical system. Left: front view of driving unit. Right: back view of bioreactor chamber (6) sockets for copper wires, (7) cam (eccentric disk), (8) follower pin, (9) plastic cantilever, (10) driving shaft (corresponding to #4 in Fig. 1A), (11) copper wires. Dashed arrows indicate spatial correspondence for assembly (see Fig. 1D for assembled bioreactor). The openings through which driving shaft and copper wires exit the bioreactor also serve as ventilation holes to allow gas exchange. **(C)** Photograph of assembled bioreactor, front right view. **(D)** Bioreactor chamber engaged to driving unit. Auxiliary parts removed to show the coupling between the bioreactor chamber and the driving unit. Notice the spatial relationship between (7) cam (eccentric disk), (8) follower pin, (9) plastic cantilever, (10) driving shaft, and (11) copper wires.

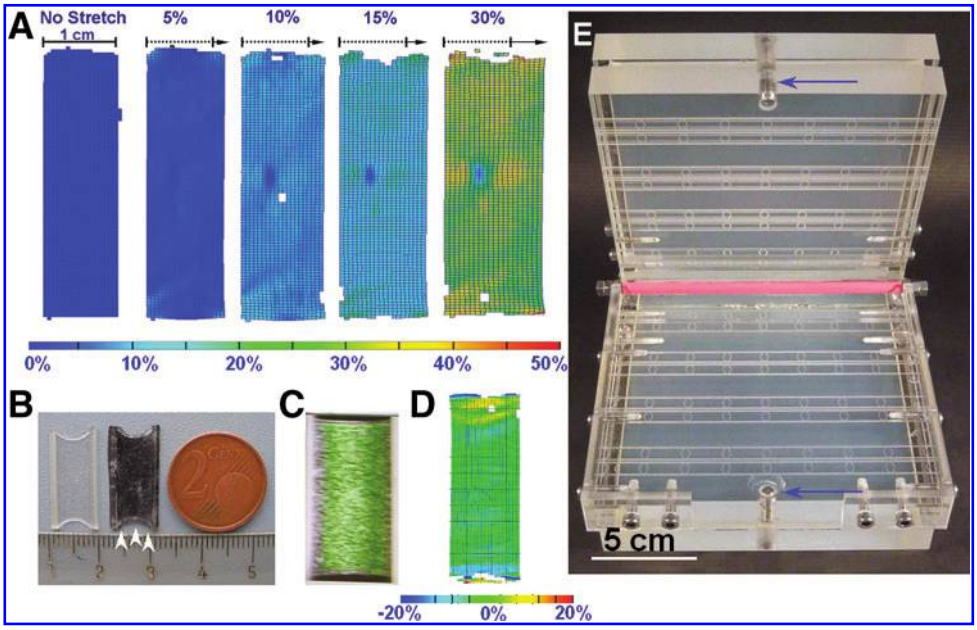

Driving system. The driving system comprises the cam coupled to a stepper motor and its control box. The characteristics of the cyclic stretch motion can be determined by the following components of the cam profile: the magnitude of stretch, that is, percent strain, is dictated by the radius of prime circle, the ratio of prime radius to base radius controls the duration of stretch relative to relaxation. The cam is coupled to a stepper motor (ST2018L0804; Nanotech Munich) driven by a custom-made control box with rotation speed ranging from 15 to 240 revolutions/min (0.25–4 Hz).

Electrical stimulation system. Based on the literature,[14] we have selected carbon rod (0.5 mm diameter, 5 cm long; Carbonteam) electrodes to be embedded to the plastic brackets in an antiparallel configuration. The opposite ends of the carbon electrodes are tied to the plastic brackets with medical suture (Fig. 4E). The carbon electrode-copper wire connecting point was cuffed with heat shrink tubing and subsequently glued with silicone adhesive to ensure proper insulation of metal wires from the culture solution. The electrodes were placed as close to the silicone polymer substrate as possible so that the electrical field stimulation is uniform.[15] Copper wires (Fig. 1B, D #11) link the electrodes to two sockets (located on the outer casing of the stepper motor, Fig. 1B #6), which can be connected to an external electrical stimulator by a 2-mm banana plug.

Methods of Analysis and Cell Culture

To assess the performance of the prototype, we characterized surface strain distribution, electrochemical impedance, and charge transfer as well as biocompatibility. The efficacy of the entire bioreactor system was validated using human umbilical cord vein cells, cardiac fibroblasts, and adult rat ventricular cardiomyocytes.

Engineering analyses

Surface deformation. To verify that desired stretch can be effectively delivered to the cultured cell monolayer, surface deformation of the PDMS substrate was analyzed using the ARAMIS system (GOM). ARAMIS is a photogrammetric technique that uses digital cameras to recognize the surface structure, and subsequently correlate these surface structures to image pixels. By capturing images from the undeformed and deformed surfaces, the displacement gradient of individual image pixels can be measured, and the ensuing surface deformation map can be constructed. However, a typical PDMS substrate is nearly transparent with minimal surface features; thus, we placed medicinal grade charcoal powder (Medizinishce Kohle, 3820M-01228; Klinik-Apotheke, University Hospital of TU Dresden) on the PDMS substrate to enhance contrast (Fig. 2B). The carbon powder-coated PDMS substrate was mounted into the bioreactor chamber, and stretch was induced by displacing the plastic bracket by a desired distance with calibrated metal inserts (resting distance between brackets = 1 cm, 5% stretch = 0.5-mm displacement, 10% stretch = 1 mm, etc.) Measured deformation for the entire surface of the PDMS substrate (Fig. 2C) was consequently analyzed and expressed as a set of color codes, from dark blue representing no deformation to orange-red corresponding to 50% elongation.

Electrochemical impedance spectroscopy. To investigate the charge transfer characteristics of the electrical stimulation system, electrochemical impedance spectroscopy (EIS) measurements were performed.[14] In brief, the bioreactor chamber was filled with the cell culture medium (Dulbecco's modified Eagle medium [DMEM]; Gibco 22320 + 10% fetal bovine serum [FBS] + 1% pen./strep.), and the electrodes were connected to a Zahner workstation (Zahner-Elektrik). With perturbation amplitudes (sinusoidal input voltages) of 10 mV, 200 mV, 500 mV, 1 V and 2 V, EIS spectra were acquired over frequencies ranging from 10^{-2} to 10^{6} Hz. EIS measurements were carried out three times, and collected data points were evaluated with Prism software to generate Bode (impedance vs. frequency) and Nyquist (real vs. imaginary components of impedance) plots. To provide insight to the behavior of the electrical stimulation system, EIS data were fit into an equivalent Randles circuit and circuit element parameters were generated in Zview software.

Charge injection/recovery. In electrical stimulation systems where electrodes are placed in physiological solutions, the charge transfer processes at the electrode/solution interface can be categorized into two major mechanisms. One is nonfaradaic reactions, which account for the simple redistribution of naturally occurring charged species, and no electron transfer between the electrode and electrolyte is associated with this process; the other mechanism, faradaic reactions, involves electron transfer at the electrode/electrolyte double layer, which results in oxidation/reduction reactions. Faradaic reactions can be further classified into two types: reversible and irreversible reactions.[16] While both nonfaradaic and reversible faradaic reactions are desirable modes of charge transfer, irreversible faradaic reactions should be preferably minimized, because they would lead to net accumulation of harmful electrochemical reaction products and degradation of electrodes.

We assessed the prevalence of irreversible faradaic reactions in the overall charge transfer scheme of the bioreactor's electrical system by measuring the amount of unrecovered charge in proportion to the total injected charge.[15,17] The bioreactor chamber was filled with the cell culture medium as in EIS studies. In 5 s, we applied a train of nine square pulses (5 and 7 V) in combinations with different duration (2, 4, and 6 ms) to our electrical stimulation system (0.5-mm-diameter, 5-cm-long carbon rods, 1 cm apart), the input voltage and duration parameters were selected based on conditions found in our laboratory to excite embryoid bodies and isolated rat cardiomyocytes. Current recordings were acquired at 10 kHz by a Zahner workstation. Each experiment was repeated nine times.

Cell isolation and culture

Biocompatibility/cell proliferation studies HUVEC. HUVEC were isolated as described previously.[18] In brief, postpartum human umbilical cord veins were washed with the M-199 medium, filled with the collagenase solution (Worthington Biochemical; 0.5 mg/mL in phosphate-buffered saline [PBS]), incubated in 37°C for 12 min. The cell-containing solution was centrifuged, resuspended in the Promocell medium (Promocell), and cultured in the T-25 flask for 3–5 days.

Confluent HUVEC were trypsinized and seeded on PDMS substrates for cyclic stretch treatment. To facilitate cell attachment, PDMS substrates were coated with fibronectin (0.1%, F1141; Sigma) and type I collagen (3 mg/mL, PureCol, 5409; INAMED) mixture (1:100 vol/vol in ddH_2O) for 4 h before seeding. After an initial plating period of 12 h during which cell attachment was confirmed by visual inspection, the bioreactor chambers were filled with 8 mL of culture medium, transferred to a standard cell culture incubator, and cyclic stretch (10%, 1 Hz) was applied for 24 h at 37°C. Two cell-seeded substrates were stretched for each experiment, and two others were placed in the bioreactor without stretch to serve as negative controls. Cells grown in T 25 flasks were taken as positive controls. All cells were stained with the proliferation marker Ki-67 (1:200 dilution; Dako) according to the manufacturer's protocol, and imaging analysis of Ki-67 versus 4',6-diamidino-2-phenylindole (DAPI) signal intensity, in terms of pixels, was performed with ImageJ software. Seven independent experiments were performed.

MTT assay and cell alignment analysis with human atrial fibroblasts. Human atrial fibroblasts were isolated by an outgrowth method.[19] Right atrial appendages were obtained from patients undergoing open heart surgery (approved by the Ethics Committee of the medical faculty of Dresden University of Technology). Biopsies were washed with PBS three times, cut into 1-mm^3 pieces under a microscope, and subsequently transferred to a Nunclon cell culture dish (60 mm; Cat#150288). About 1 mL of the fibroblast medium (DMEM, 1 g/mL glucose, supplemented with 10% FBS and 1% pen./strep.) was slowly dripped over the biopsies. Subsequent medium change was carried out every other day. In approximately 3 days, early signs of adherent cell outgrowth could be observed. Cells were confluent in the vicinity of most biopsies after 2 weeks. Outgrowth cells showed an elongated, spindle-shaped morphology characteristic of fibroblasts, and their identity was subsequently confirmed with positive vimentin and human fibroblast surface antigen staining and negative for smooth muscle myosin heavy chain. Cells were harvested by standard trypsin treatment and seeded on the PDMS polymer substrate. Cyclic stretch (10%, 1 Hz for 24 h) was applied as described for HUVEC. Two cell-seeded PDMS substrates were stretched for each experiment, and two others were placed in the bioreactor without stretch to serve as negative controls. At the end of each experiment, five microscopic images were taken for each substrate at 10× magnification, and cell alignment analysis was performed on 10 randomly selected cells from each image using the angle tool of ImageJ software. The cell angle was defined as the angle between the cell's longitudinal axis and the direction of stretch, for example, if a cell aligned perpendicular to stretch, the cell angle would be recorded as 90°. Cell alignment experiments were performed three times on 300 atrial fibroblast cells isolated from three different patients.

MTT (3-[4,5-dimethyl-thiazol-2-yl]-2,5-diphenyltetrazolium bromide; V13154, Sigma) assay was performed to assess cytotoxicity. Equal number (2.0×10^4 cells per substrate/well) of human atrial fibroblasts was seeded on PDMS substrates and 24-well plates (Nunclon, Cat#142475), both of which have an effective growth area of 2 cm^2. Two PDMS substrates were subjected to cyclic stretch (10%, 1 Hz). Two other cell-seeded substrates placed in a bioreactor without stretch. Cells cultured on 24-well plates were used as a positive control. After 24 h of cultivation, PDMS substrates were transferred from the bioreactor onto a Nunclon cell culture dish (60 mm, Cat#150288). For all three conditions (stretch, no stretch, and 24-well plate), cells were washed three times with PBS. The normal Tyrode's solution (200 μL) containing 1.2 mM MTT was loaded onto PDMS substrates and 24-well plates. Cells were then incubated at 37°C for 4 h, during which the yellow water-soluble MTT salt was reduced into violet-blue water-insoluble formazan by viable cells. Formazan was subsequently dissolved by 50 μL of dimethyl sulfoxide, and the optical density was measured at 540 nm using an ND-1000 NanoDrop® Spectrophotometer (NanoDrop Technologies). Each sample was measured three times, and three independent experiments were performed in duplicates.

Contractile characteristics of rat ventricular myocytes under field stimulation. To compare the efficacy in delivering field stimulation between the bioreactor and a standard stimulation device, rhythmic contractions were triggered in isolated rat ventricular myocytes by field stimulation. Briefly, ventricular myocytes were isolated from male Wistar rats ($n=4$, weighing about 150 g) as described previously.[20] Isolated cells were stored in a storage solution for up to 6 h at room temperature until use. The stimulation chambers were prefilled with a fresh normal Tyrode's solution before each experiment, and mounted to an inverted microscope coupled with a Soft-edge Myocam system (Ionoptix) at room temperature (Fig. 6A). To record the contractile response, rat ventricular myocytes were loaded on to the PDMS substrate (carbon electrodes 1 cm apart) or a standard field stimulation chamber (RC-21BRFS; Warner Instruments), and allowed to settle down. Fluid perfusion, driven by a peristaltic pump (0.6 mL/min, Minipuls 3; Gilson) and vacuum suction (Fig. 6A), was turned on and remained flowing through each recording. Contractions were excited with 7 V/cm, 4 ms bipolar pulses at 1 or 2 Hz (STIM; SI Heidelberg), and alternating recordings were performed with the bioreactor chamber and the standard field stimulation chamber. Each recording typically lasted 3–5 min. Contractile parameters, including peak shortening, time to peak tension (TPT), and time to 50% relaxation (TR50), were used to compare the efficacy of the two chambers.

Statistical analysis

Charge injection/recovery studies were analyzed by one-way analysis of variance with the Bonferroni's multiple comparison test. Ki-67 and MTT signals were analyzed using the paried *t*-test to evaluate cytotoxicity. The Student's *t*-test was used to compare contractile characteristics of rat cardiomyocyte shortening in bioreactor versus standard field stimulation. The Shapiro-Wilk normality test was used to assess whether angles of fibroblast cell alignment were consistent with the Gaussian distribution, and the *f*-test was used to compare the variances of stretched versus control. Statistical significance was considered at $p<0.05$. Graph Pad Prism 5 software was used to conduct all statistical analyses.

Results

Surface strain analysis and cell responses to stretch

Surface strain analysis is depicted in Figure 2A. As the PDMS substrate is stretched up to 30% with 5% increments,

FIG. 3. Cell response to stretch. **(A)** Proliferation marker Ki-67 staining of human umbilical vein endothelial cells (HUVEC). Scale bar = 25 μm. Sample image from: left, positive control, cells in conventional culture flask. Center, bioreactor chamber without stimulation. Right, bioreactor with 1 Hz stimulation for 24 h. Pink: Ki-67 signal. Blue: 4′,6′-diamidino-2-phenylindole nucleus (DAPI). **(B)** Cell alignment in response to cyclic stretch. Sample photographs of nonstretched control (left) and stretched human atrial fibroblasts (right). While control group showed cells aligned randomly, stretched group aligned perpendicular to the direction of stretch, which is indicated by the white arrow. **(C)** Angle of alignment analysis. As demonstrated in the inset of the left figure, angle of alignment is defined as the angle between the direction of stretch and the left end of the cell's longitudinal axis. Control group (left) shows a uniform distribution, whereas the majority of stretched cells aligned 90° with respect to the direction of stretch (right). Each bar graph represents cumulative results obtained from 300 cells in three independent experiments in duplicates. *f*-Test indicated the variance in stretched group is significantly smaller than control ($p < 0.0001$). Shapiro-Wilk test revealed the alignment angle data from control is inconsistent with Gaussian distribution ($p < 0.0001$), whereas the null hypothesis (i.e., alignment angle samples come from a normally distributed population) cannot be rejected in stretched group ($p = 0.5469$). **(D)** Proliferation marker analysis from HUVEC. Averaged signal intensity ratio of Ki-67 versus DAPI ($n = 7$). Samples from all three groups displayed similar levels of Ki-67 signal normalized to DAPI, and no statistical difference was found among these data. **(E)** (3-[4,5-dimethyl-thiazol-2-yl]-2,5-diphenyltetrazolium bromide (MTT) assay from human atrial fibroblasts ($n = 6/3$). Samples from bioreactor without stretch and conventional culture dish displayed similar levels of MTT signal, whereas stretch treatment resulted in significantly increased MTT signal compared to control ($^*p < 0.05$).

measured surface deformation is consistent with applied stretch. Color distribution across the entire surface of the substrate is uniform, indicating the homogeneity of stretch in the system.

Biocompatibility of the bioreactor chamber, was assessed by measuring proliferation of HUVEC and MTT signals in human atrial fibroblasts subjected to cyclic stretch for 24 h. Fluorescent microscopy images (Fig. 3A) revealed signals for Ki-67, indicating a considerable population of HUVEC were actively proliferating in bioreactor chambers with and without cyclic stretch as well as in conventional cell culture flasks. The highest proliferation signal intensity was found in the stretched group, but such an increase was not statistically significant (Fig. 3D, $n = 7$). In human atrial fibroblasts, MTT signals were similar in the positive control (24 h cultivation on 24-well plate) and cells grown in the bioreactor without stretch, indicating the materials used to build the bioreactor are not cytotoxic. Fibroblasts subjected to 10% stretch at 1 Hz for 24 h exhibited a significantly increased ($p < 0.05$) level of MTT signal, suggesting cell proliferation or an elevated mitochondrial activity in the stretched group (Fig. 3E). The efficacy of the mechanical stimulation was confirmed by cell alignment under cyclic stretch, a well-established biological response in fibroblasts.[21] Human atrial fibroblasts seeded on PDMS substrates without stretch exhibited an elongated, spindle-shaped morphology with random orientation indistinguishable from those grown in conventional cell culture flasks (Fig. 3B). After 24 h of cyclic stretch, most aligned perpendicular to the direction of stretch (Fig. 3B, C, and Supplementary Movie S3). The Shapiro-Wilk test reveals that the measured angles alignment in nonstretched cells are inconsistent with the Gaussian distribution, and the *f*-test shows the variance in the nonstretched group is significantly higher than stretched cells ($p < 0.0001$ for both tests), indicating the randomness in cell orientation without stretch.

Characterization of electrical stimulation system and contractile response

Electrochemical impedance spectroscopy. Bode and Nyquist plots generated from EIS measurements are shown in Figure 4. At a certain input voltage, the magnitude of the entire bioreactor's impedance decreases as the frequency increases, and the higher input voltage is associated with a lower impedance (Fig. 4A), which is also reflected in the Nyquist plot (Fig. 4C). Moreover, the Bode plot of phase

FIG. 4. Electrochemical impedance spectroscopy (EIS) results and equivalent circuit analysis. Bode plots of magnitude **(A)** and phase angle **(B)** of the overall impedance of the entire bioreactor electrical stimulation system as a function of input voltage and frequency. Nyquist plots **(C)** were subsequently constructed to represent the relationship between real versus imaginary parts of impedance. A zoomed-in Nyquist plot [**(C)**, inset] is provided to show the details for data obtained from higher voltages. The color code is valid for all three figures. Bode and Nyquist plots are taken from one representative experiment. The electrochemical behavior of the bioreactor's electrical system can be modeled with a Randles circuit [**(D)**, top], in which Rs corresponds to the resistance of the bulk solution, Rp stands for the polarization resistance, that is, resistance to corrosive electrochemical reactions, and $C_{\text{double-layer}}$ represents the capacitance of the electrode/solution double layer. In reality, however, the actual nonlinear behavior of this virtual capacitor can be more accurately modeled as a constant phase element (CPE), which acts like a mixture of resistor and capacitor, as shown in the modified Randles circuit [**(D)**, bottom]. Therefore, we report its magnitude as CPE and ideality fraction η as its linearity, ranging between 0 and 1, where 0 represents a pure resistor and 1 means a pure capacitor. **(E)** Bottom view of bioreactor chamber: white arrows indicate carbon rod electrode (only one shown, the other hidden behind the plastic clamp on the opposite side). Electrodes are fixed to plastic clamps by medical sutures (green arrows). Such design minimizes distance between electrodes, thereby maximizes field strength of electrical stimulation. **(F)** Equivalent circuit analysis. Three independent EIS experiments were performed on three fresh pairs of electrodes for equivalent circuit analysis. Graphs represent average values ± standard error of the mean (SEM). Left, while Rs did not show any appreciable change, R_p value decreased dramatically as input voltage increase from 10 to 500 mV and leveled off at 1 V and 2 V. Right, CPE value increased and η decreased at input voltages from 10 mV to 2 V. Notice that the error bars here, representing SEM, is conceptually different from deviation in Table 1. SEM depicts the variance from one measurement to another, whereas deviation accounts for the difference between the actual measured values and calculated results from modeling. Deviation signifies how well the Randles cell model can fit the experimentally acquired data.

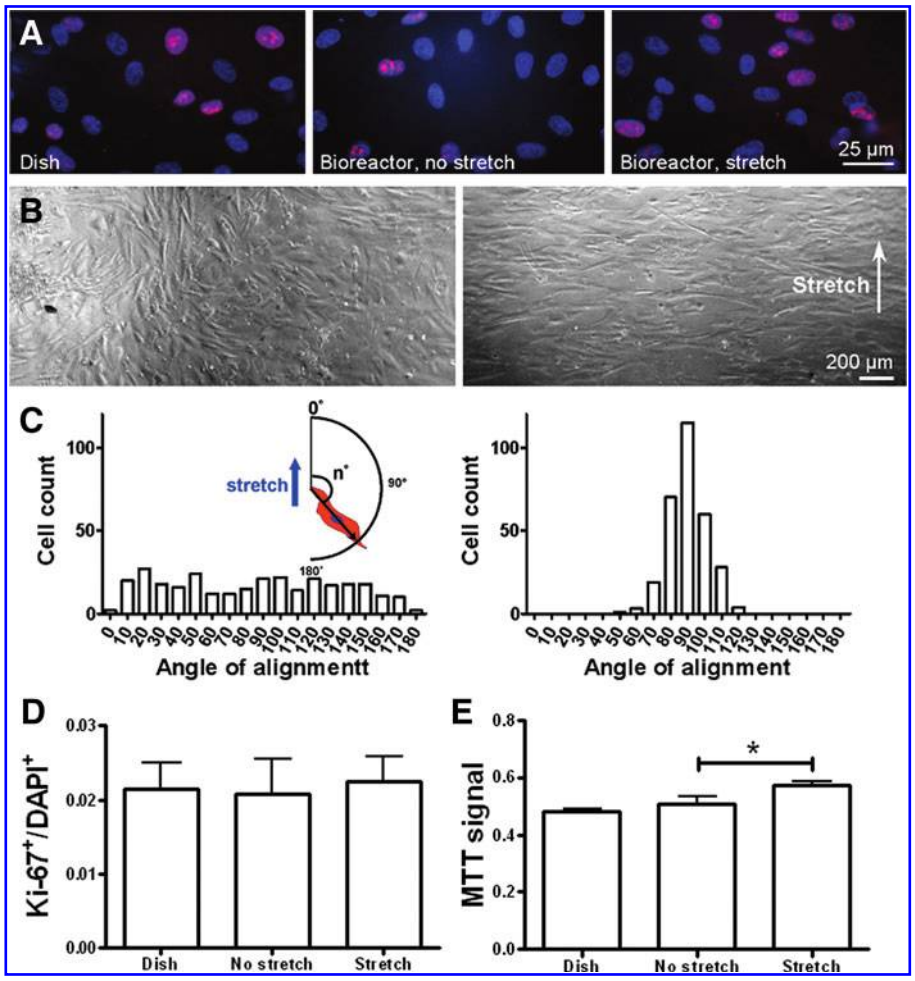
A
Dish
Bioreactor, no stretch
Bioreactor, stretch
25 μm
B
Stretch
200 μm
C
Cell count
stretch
n°
0°
90°
180°
Angle of alignmentt
Angle of alignment
D
Ki-67+/DAPI+
Dish
No stretch
Stretch
E
MTT signal
*
Dish
No stretch
Stretch

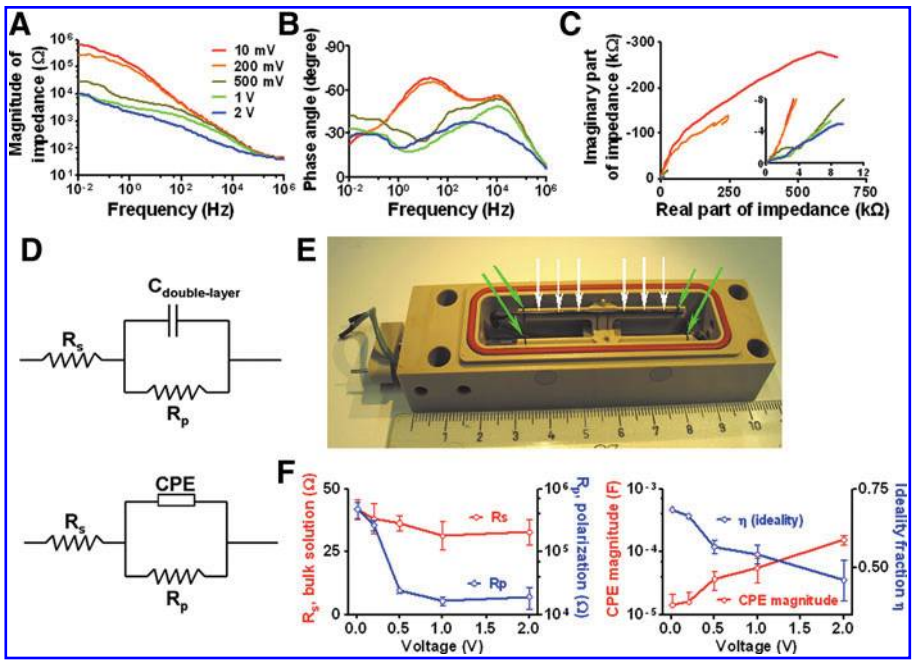
A
Magnitude of impedance (Ω)
10 mV
200 mV
500 mV
1 V
2 V
Frequency (Hz)
B
Phase angle (degree)
Frequency (Hz)
C
Imaginary part of impedance (kΩ)
Real part of impedance (kΩ)
D
C double-layer
Rs
Rp
CPE
Rs
Rp
E
F
Rs, bulk solution (Ω)
Rp, polarization (Ω)
Rs
Rp
Voltage (V)
CPE magnitude (F)
η (ideality)
CPE magnitude
Ideality fraction η
Voltage (V)

angle versus input frequency (Fig. 4B) reveals that higher input voltages tend to yield lower phase angles, suggesting a reduction in the capacitive component and elevation in the resistive component of overall impedance, which is mirrored by the gentle slope in the Nyquist plot (Fig. 4C).

The data acquired from EIS experiments were fit into an equivalent Randles circuit (Fig. 4D, top), in such an *in silico* model, each parameter of the circuit elements can be used to assess the physical property of the electrical stimulation system, for instance, R_s corresponds to the resistance of the bulk solution, R_p stands for the polarization resistance, that is, resistance to corrosive electrochemical reactions, and $C_{double\text{-}layer}$ represents the capacitance of the electrode/solution double layer. The actual nonlinear behavior of this virtual capacitor can be more accurately modeled as a constant phase element (CPE), which acts like a mixture of resistor and capacitor. Therefore, we report its magnitude as CPE and its linearity as an ideality fraction η, ranging between 0 and 1, where 0 represents a pure resistor and 1 means a pure capacitor.

The EIS experiments were performed three times using a fresh set of electrodes each time, and the averaged parameters and percent deviation, defined as the difference between the actual collected data and calculated theoretical values, are shown in Table 1.

Calculated equivalent circuit parameters were subsequently analyzed as a function of input voltage. While the resistance of the bulk solution did not show any appreciable change, the polarization resistance exhibited a sharp decrease as the input voltage increased from 10 to 500 mV, and then leveled off at higher voltages (Fig. 4E). Moreover, with the increasing input voltage, CPE showed a steady increase, suggesting elevated overall impedance, and η decreased, indicating a decline in the capacitive property of at the electrode-solution double layer (Fig. 4F). Figure 4E and F show averaged results from three experiments; error bars represent standard error of the mean, which accounts for the variance from experiment to experiment.

Charge injection/recovery. As shown in the original voltage and current tracings (Fig. 5A), by applying 5 V, 2 ms pulses, current flow could be detected in the bioreactor system (Fig. 5B). Immediately after the application of the pulse, a transient, reverse current flow could be detected. The amounts of injected (Fig. 5C, hatched) and recovered charge (Fig. 5C, dotted) were calculated by integrating current over time with custom-written Matlab (MathWorks, Inc., Natick, MA) script. Injected charge was integrated over the respective duration of each pulse, and recovered charge was integrated over 30 ms, in which the reverse current flow reached a steady state. The unrecovered percentage ratio was calculated by the formula: (1 − recovered charge/injected charge)×100.

As input voltage varies in combinations with different pulse duration, 5 V, 2 ms pulses had the smallest unrecovered ratio; with a higher input voltage and a longer pulse duration, an increasing proportion of the injected charge was left unrecovered, with 5 V, 6 ms pulses, roughly half of the injected charge was not recovered due to irreversible faradaic reaction, and the highest voltage (7 V) in combination with the longest duration (6 ms) rendered over three quarters of the injected charge unrecovered (Table 2). As shown in Figure 5D, with the exception of three pairs of data sets (5 V/2 ms vs. 5 V/4 ms, 5 V/4 ms vs. 5 V/6 ms, 7 V/4 ms vs. 7 V/6 ms), the difference between any two given sets of data is statistically significant.

Cell shortening of rat cardiomyocytes under field stimulation: comparative contractile characteristics. Field stimulation delivered through the bioreactor's electrical stimulation system could evoke a contractile response at 1 and 2 Hz (Fig. 6C). Compared to contractions obtained from cells stimulated by a standard Warner chamber, the bioreactor could induce a significantly higher peak shortening at 1 Hz, but not 2 Hz (Fig. 6D). Other parameters, including TPT and TR50, are also similar (Fig. 6E, F).

Discussion

In this study, we designed, constructed, and validated a bioreactor system to provide cyclic stretch, electrical stimulation, and constant perfusion to cultured cells.

To address the native dynamic environment of the cardiac niche, various cyclic stretch bioreactor systems have been developed.[22,23] One commercially available and widely used device is Flexcell (Flexcell International). In Flexcell, the strain of cell culture substrate is achieved by applying vacuum-controlled deformation along the circumference of a circular silicone membrane, yielding 2D stretch. However, due to the viscoelasticity of the silicone membrane, the pressure–strain relationship requires a unique calibration.[24] In addition, its circular stretch regime leads to inhomogeniety of the strain field,[25] and special modifications are required for stimulating strips of cardiac tissue construct.[26] Furthermore, Flexcell must be driven by a vacuum source applied to the bottom of the dish, which precludes the possibility for real-time inspection with an inverted microscope. Our system utilizes a simple

Table 1. Calculated Parameters of the Equivalent Circuit ($n=3$)

Input voltage	R_s *(Ω)*	*(% deviation)*	R_p *(Ω)*	*(% deviation)*	*CPE (F)*	*(% deviation)*	η	*(% deviation)*
10 mV	41.86	2.62	4.78E+05	5.57	1.44E−05	2.03	0.68	0.45
200 mV	38.21	2.48	2.66E+05	4.49	1.60E−05	2.04	0.66	0.46
500 mV	36.39	7.16	2.45E+04	6.42	3.70E−05	7.96	0.57	1.91
1 V	31.44	7.50	1.65E+04	9.76	5.55E−05	10.24	0.54	2.34
2 V	32.84	3.40	1.94E+04	11.73	1.57E−04	3.47	0.46	1.33

R_s simulates the solution's resistance, R_p is a measure of the electrode's resistance to electrochemical corrosion, CPE stands for the magnitude of the nonlinear capacitance and η denotes the linearity of the CPE element ($\eta=1$ for an ideal capacitor, decreases as the CPE behaves in a more resistive and less capacitive manner). Percent deviation shows the difference between the measured and theoretical values, hence, indicates how well the computer generated equivalent Randles circuit model can describe the actual behavior of the electrical stimulation system of the bioreactor.

CPE, constant phase element.

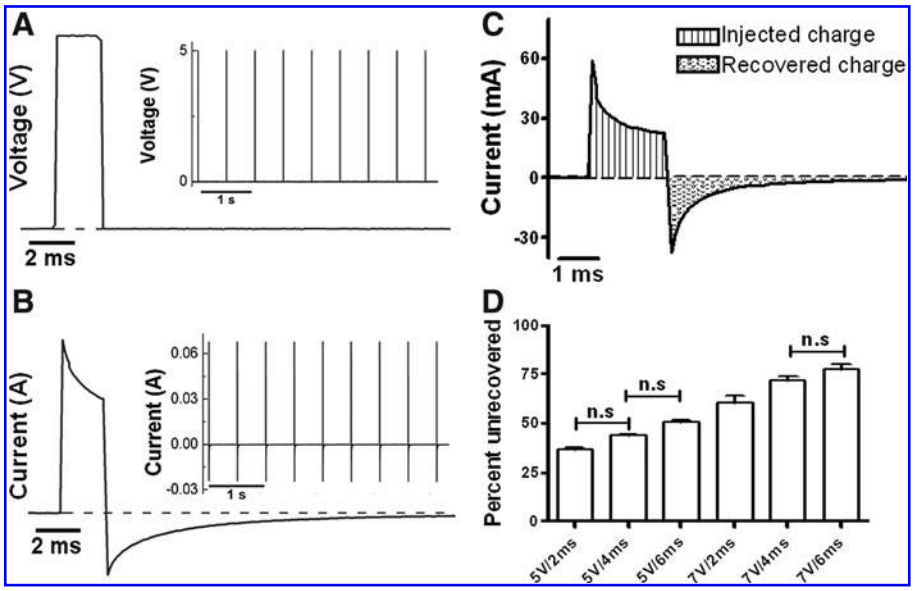

FIG. 5. Charge injection/recovery study. **(A)** Input voltage protocol, expanded image to show the characteristics of one applied voltage pulse. For each experiment with each set of voltage/pulse duration parameters, a train of nine square pulses (inset representative of 5 V, 2 ms protocol) was applied to culture medium-filled bioreactor chamber. **(B)** Original current tracings, expanded image to show the characteristics of measured current flow in response to the applied voltage pulse. Inset shows a train of current pulses resulting from the input voltage train. The time axes of **(A)** and **(B)** are aligned to show the time-variant characteristics of each recording. Immediately after the termination of the voltage pulse, a current flow in the reverse direction could be detected. Current flowing into the system is arbitrarily recorded as positive values, and negative values represent current flow in the reverse direction, which corresponds to charge recovery due to reversible mechanisms. **(C)** Sample current-versus-time tracing, demonstrating the concept of calculating injected charge and recovered charge by integrating current over time. Area under the curve and above the horizontal axis (hatched) corresponds to injected charge, whereas area below axis and above the curve (dotted) denotes recovered charge due to reversible mechanisms. **(D)** Percentage ratio of unrecovered charge versus input voltage parameters. With higher pulse amplitude (5–7 V) and duration (2, 4, and 6 ms), increasing proportions of charge were not recovered. The difference between any two given columns is statistically significant unless otherwise labeled (n.s.). Results obtained from nine experiments performed on three sets of fresh electrodes.

motor/cam/shaft mechanism, which allows the application of homogeneous, uniaxial stretch to culture cells (Fig. 2A). Stretch parameters, including percent strain and relative duration of stretch versus relaxation within one cycle are determined by the cam profile. Moreover, the cam can be designed for either shortening or elongation to mimic cycles of contraction or extension as required for myocardium or the lung and aortic valve, respectively. The compact design of our system also allows inspection using a standard microscope (Supplementary Movies M3 and M4). With the custom-made polycarbonate casting mold, it is foreseeable that 3D tissue constructs (e.g., cardiomyocytes suspended in fibrin or collagen gel) can be made with the same shape as the PDMS substrates, so that this bioreactor system should be compatible with 3D applications without major modification.

We have demonstrated the biocompatibility of the device with proliferation/cytotoxicity experiments. Endothelial cells and fibroblasts are the major auxiliary cell populations in the myocardium, and cardiac regeneration studies have indicated their roles in promoting the structural and functional development in tissue constructs.[27,28] We reason that they are among the potential cell populations to be used in this device, therefore, we used HUVEC and cardiac fibroblasts to test the device's biocompatibility. HUVEC grown in the bioreactor,

Table 2. Charge Injection/Recovery Under Various Stimulation Parameters (n=9)

		5 V, 2 ms	*5 V, 4 ms*	*5 V, 6 ms*	*7 V, 2 ms*	*7 V, 4 ms*	*7 V, 6 ms*
Injected charge (μC)	Mean	44.59	70.05	91.10	92.69	182.70	271.00
	SEM	3.15	5.92	6.98	1.61	2.16	2.32
Recovered charge (μC)	Mean	27.90	39.56	45.15	36.54	51.95	60.05
	SEM	1.95	3.56	4.21	3.47	4.91	5.73
Unrecovered percentage	Mean	36.51	43.44	50.83	60.91	71.72	77.95
	SEM	1.33	0.48	0.79	3.01	2.35	1.91

Averaged values from nine experiments performed on three sets of electrodes. Injected charge denotes the amount of charge being delivered into the cell culture solution as a result of the applied voltage pulse. Recovered charge indicates how much charge could be regained by the electrodes due to reversible mechanisms. Unrecovered percentage signifies the averaged proportion of lost charge for each voltage pulse, which is correlated to corrosive damage of carbon electrodes.

SEM, standard error of the mean.

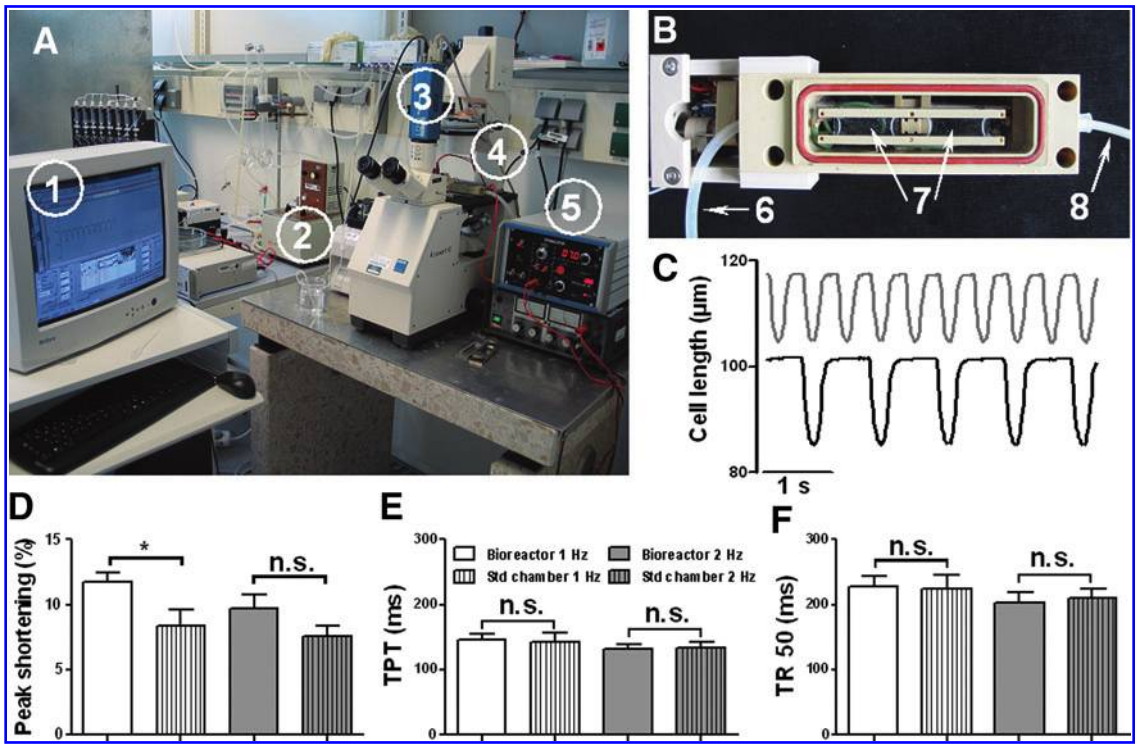

FIG. 6. Cell shortening of rat ventricular myocytes under field stimulation. **(A)** Cell shortening data acquisition system, consisting (1) computer, (2) peristaltic pump and fluid reservoir of normal Tyrode's solution in a beaker, (3) Myocam camera, (4) bioreactor chamber, and (5) voltage source. All recordings were done at room temperature. **(B)** Bottom view of bioreactor. (6) rubber tubing to vacuum suction, (7) PDMS substrates clamped in bioreactor chamber and (8) rubber tubing from peristaltic pump. **(C)** Representative original tracings of cell shortening in response to field stimulation delivered through the bioreactor's electrical stimulation system. Black, 1 Hz, and gray, 2 Hz. **(D)** Peak cell shortening, as a percentage of original cell length. Adult rat ventricular myocytes under 7 V/cm, 4 ms field stimulation delivered through bioreactor chamber exhibited increased peak shortening at 1 Hz compared to those in standard chambers. Averaged peak cell shortening values are rather similar between these two groups at 2 Hz. Other contractile parameters, including time to peak tension **(E)** and time to 50% relaxation **(F)** are also comparable. These similarities suggest the bioreactor's efficacy in delivering field stimulation is commensurate with a standard device. Cell shortening data were obtained from 11 to 13 cells from three independent isolations for each column. Each recording typically lasted for 3–5 min (n.s. = not significant, $*p < 0.05$). Color images available online at www.liebertpub.com/tea

regardless of cyclic stretch treatment, exhibited proliferation signals comparable to those in the conventional culture flask as evidenced by Ki-67 staining (Fig. 3A). These results indicate that the bioreactor, in particular, cyclic stretch applied through this system, does not impose adverse effect on HUVEC proliferation. In human atrial fibroblasts, however, cyclic stretch treatment significantly enhanced the MTT signal, which is consistent with the previous study in tendon fibroblasts.[29]

It was reported that the human skin fibroblast align about 60° to the direction of stretch.[30] This discrepancy can be attributed to difference in the substrates, namely, our PDMS substrates were designed to counterbalance the Poisson effect, so that the lateral strain is arguably negligible as evidenced by ARAMIS strain maps (Fig. 2D). Human atrial fibroblasts showed a normal distribution of alignment angles centered at 90° relative to the direction of stretch, as predicted by Wang's mathematical models.[31] This behavior is thought to minimize the cells' exposure to substrate deformation.[32] Although this validation study confirms the bioreactor's efficacy in delivering cyclic stretch to cultured cells, the mechanical properties of this system, especially the interplay between the geometry of the PDMS substrate and the surface strain distribution, warrant further investigation.

Surface activation to facilitate cell attachment to the hydrophobic PDMS substrate was achieved by coating with fibronectin/collagen diluted in water. Our original approach involved low-pressure NH_3 plasma treatment followed by poly(ethylene glycol) linkage for surface adsorption of fibronectin, collagen, and gelatin. We later discovered that directly coating the PDMS substrate with fibronectin and collagen diluted in water was sufficient to allow cell attachment. Due to the hydrophobicity and rapid recovery to a hydrophobic state after hydrophilization, PDMS surface modification techniques demand more rigorous investigation,[33] and the mechanism for this fibronectin/water-based PDMS surface modification, especially its efficacy for long-term applications, remains to be tested.

EIS was used in this study to characterize the electrical stimulation system. In Bode and Nyquist plots, the overall impedance decreased with a higher input voltage, suggesting increasing levels of corrosion at the carbon electrode–culture solution double layer; in particular, analysis with equivalent Randles circuit showed voltage-dependant variations in polarization resistance, magnitude, and ideality fraction of the CPE (Fig. 4). These results point to corrosive damage at the surface of carbon electrodes due to a higher input voltage. Equivalent circuit analysis also revealed the impedance at the electrolyte–electrode interface exceeds the impedance of the cell culture solution by over three orders of

magnitude (Fig. 4E), suggesting opposition to current flow predominately occurs at the electrolyte–electrode interface. Thus, varying the distance between electrodes due to cyclic stretch would impose diminutive influence on the overall electrochemical property of the bioreactor system.

From equivalent circuit analysis, we noticed a trend in polarization resistance (R_p, Fig. 4F); namely, the R_p value decreased dramatically as the input voltage increased from 10 to 500 mV and leveled off at 1 and 2 V. We postulate that this trend might be attributed to a voltage threshold to mobilize the neutral species to become charge carriers, similar to the concept of ionization energy. At lower input voltages, the naturally occurring charged species are sufficient to facilitate the energy transfer process. However, as the input voltage increases, additional charge carriers must be generated at the carbon electrode surface and within the solution to accommodate for a greater demand. Once this threshold voltage is reached, an abundance of charged species could be generated at the electrode/electrolyte double layer and within the solution, resulting in a flat curve of R_p at 1 and 2 V.

Previous studies provided guidance on electrical stimulation parameters, electrode material selection, and configuration.[14,15,17] Charge injection/recovery studies with the same stimulation parameters (5 V, 2 ms) revealed that the unrecovered charge ratio in our system is more than two-fold higher than the value from Tandon *et al.*'s study,[15] perhaps, due to difference in the geometry of stimulation chambers, sizes of carbon electrodes, and solutions. These results point to the balance between two factors in the electrical stimulation system for biological applications, that is, corrosive damage can be reduced by lowering the stimulation voltage and shortening pulse duration, but stimulation strength must be large enough to provoke biological responses.

The bioreactor's electrical stimulation system was validated by eliciting rhythmic contractions in rat cardiomyocytes with regular field stimulation from an external voltage stimulator. It was reported that, under the current injection mode, the cardiomyocyte contraction is triggered by a sodium ion channel-dependent mechanism as in a normal action potential, whereas voltage stimulation results in contraction via the direct activation of L-type calcium channels and the sodium–calcium exchanger.[34] Given the fact that injected current determines the amount of electrical field applied to cells in a bioreactor system,[14] we reason that the current source is a better alternative, in the sense of being a closer condition to the physiological cascade of excitation–contraction coupling, over voltage stimulators.

The bioreactor's perfusion system was only tested in field stimulation experiments to demonstrate that the fluid inlets and outlets, along with a peristaltic pump and vacuum suction, can provide a functional mechanism for constant fluid exchange. One limitation of our study is that field stimulation experiments only lasted for 10 min at most, which are definitely too short for cardiac conditioning applications. Furthermore, we tested a slow perfusion rate of 0.6 mL/min, so that settled rat ventricular myocytes were not washed away. As pointed out by Carrier *et al.*'s study, cardiac tissue constructs showed noticeable improvements after 10 days of perfusion at 3 mL/min, but not 1 mL/min or 0.6 mL/min.[10] Therefore, additional design improvements are required to further refine the current prototype for long-term experiments with a higher flow rate.

Future Work

To further optimize the system, we are currently devising an electrical stimulation apparatus for current injection and implementing an optical sensor to synchronize cyclic stretch and electrical stimulation. Another important area of future work is to test this device for stimulating 3D cardiac tissue. Many previous studies in tissue engineering have indicated that cyclic stretch[7,35] and continual field stimulation[8,14] can lead to functional improvement in the cardiac tissue construct. Given its capability of providing both of these stimuli, we propose this bioreactor as a potential device for cardiac tissue engineering. Furthermore, additional bioreactor chambers are under construction, so that experiments with different stimulation parameters can be carried out in an independent and simultaneous manner.

Other areas of future work include further refining the electrical stimulation regime (different cam profiles to accommodate different physiological conditions, smart waveforms of electrical stimulation to reduce corrosive electrochemical reaction, electrical–mechanical coupling mechanism to mimic pathological conditions, such as arrhythmia and the perfusion system to accommodate for long-term conditioning culture), evaluating the effect of physical stimulation on cells that reside in the cardiac niche, such as cardiomyocytes, fibroblasts, endothelial cells (angiogenesis), and macrophages (inflammation).

Acknowledgments

The authors would like to thank Dr. Konrad Schneider and Holger Scheibner for help with ARAMIS studies. This study was supported by a grant from the Fondation Leducq.

Disclosure Statement

No competing financial interests exist.

References

1. Leychenko, A., Konorev, E., Jijiwa, M., and Matter, M. L. Stretch-induced hypertrophy activates NFkB-mediated VEGF secretion in adult cardiomyocytes. PLos One **6,** 2011.
2. Tsai, C.T., Chiang, F.T., Tseng, C.D., Yu, C.C., Wang, Y.C., Lai, L.P., Hwang, J.J., and Lin, J.L. Mechanical stretch of atrial myocyte monolayer decreases sarcoplasmic reticulum calcium adenosine triphosphatase expression and increases susceptibility to repolarization alternans. J Am Coll Cardiol **58,** 2106, 2011.
3. Husse, B., Briest, W., Homagk, L., Isenberg, G., and Gekle, M. Cyclical mechanical stretch modulates expression of collagen I and collagen III by PKC and tyrosine kinase in cardiac fibroblasts. Am J Physiol Regul Integr Comp Physiol **293,** R1898, 2007.
4. Lee, A.A., Delhaas, T., McCulloch, A.D., and Villarreal, F.J. Differential responses of adult cardiac fibroblasts to *in vitro* biaxial strain patterns. J Mol Cell Cardiol **31,** 1833, 1999.
5. Berger, H.J., Prasad, S.K., Davidoff, A.J., Pimental, D., Ellingsen, O., Marsh, J.D., Smith, T.W., and Kelly, R.A. Continual electric-field stimulation preserves contractile function of adult ventricular myocytes in primary culture. Am J Physiol **266,** H341, 1994.
6. Holt, E., Lunde, P.K., Sejersted, O.M., and Christensen, G. Electrical stimulation of adult rat cardiomyocytes in culture improves contractile properties and is associated with altered calcium handling. Basic Res Cardiol **92,** 289, 1997.

7. Zimmermann, W.H., Melnychenko, I., and Eschenhagen, T. Engineered heart tissue for regeneration of diseased hearts. Biomaterials **25,** 1639, 2004.
8. Radisic, M., Park, H., Shing, H., Consi, T., Schoen, F.J., Langer, R., Freed, L.E., and Vunjak-Novakovic, G. Functional assembly of engineered myocardium by electrical stimulation of cardiac myocytes cultured on scaffolds. Proc Natl Acad Sci U S A **101,** 18129, 2004.
9. Feng, Z.G., Matsumoto, T., Nomura, Y., and Nakamura, T. An electro-tensile bioreactor for 3-D culturing of cardiomyocytes - a bioreactor system that simulates the myocordium's electrical and mechanical response *in vivo*. IEEE Eng Med Biol Mag **24,** 73, 2005.
10. Carrier, R.L., Rupnick, M., Langer, R., Schoen, F.J., Freed, L.E., and Vunjak-Novakovic, G. Perfusion improves tissue architecture of engineered cardiac muscle. Tissue Eng **8,** 175, 2002.
11. Radisic, M., Yang, L.M., Boublik, J., Cohen, R.J., Langer, R., Freed, L.E., and Vunjak-Novakovic, G. Medium perfusion enables engineering of compact and contractile cardiac tissue. Am J Physiol Heart Circ Physiol **286,** H507, 2004.
12. Radisic, M., Marsano, A., Maidhof, R., Wang, Y., and Vunjak-Novakovic, G. Cardiac tissue engineering using perfusion bioreactor systems. Nat Protoc **3,** 719, 2008.
13. Maidhof, R., Tandon, N., Lee, E.J., Luo, J., Duan, Y., Yeager, K., Konofogou, E., and Vunjak-Novakovic, G. Biomimetic perfusion and electrical stimulation applied in concert improved the assembly of engineered cardiac tissue. J Tissue Eng Regen Med **6,** e12, 2011.
14. Tandon, N., Cannizzaro, C., Chao, P.H.G., Maidhof, R., Marsano, A., Au, H.T.H., Radisic, M., and Vunjak-Novakovic, G. Electrical stimulation systems for cardiac tissue engineering. Nat Protoc **4,** 155, 2009.
15. Tandon, N., Marsano, A., Maidhof, R., Wan, L., Park, H., and Vunjak-Novakovic, G. Optimization of electrical stimulation parameters for cardiac tissue engineering. J Tissue Eng Regen Med **5,** E115, 2011.
16. Merrill, D.R., Bikson, M., and Jefferys, J.G.R. Electrical stimulation of excitable tissue: design of efficacious and safe protocols. J Neurosci Methods **141,** 171, 2005.
17. Tandon, N., Cannizzaro, C., Figallo, E., Voldman, J., and Vunjak-Novakovic, G. Characterization of electrical stimulation electrodes for cardiac tissue engineering. Abstract presented at the *Proceedings of the 28th IEEE EMBS Annual International Conference*, New York City, 2006. Abstract no. 259747.
18. Schnittler, H.J., Franke, R.P., Akbay, U., Mrowietz, C., and Drenckhahn, D. Improved in-vitro rheological system for studying the effect of fluid shear-stress on cultured-cells. Am J Phys **265,** C289, 1993.
19. Villarreal, F.J., Bahnson, T., and Kim, N.N. Human cardiac fibroblasts and receptors for angiotensin II and bradykinin: a potential role for bradykinin in the modulation of cardiac extracellular matrix.. Basic Res Cardiol **93,** 4, 1998.
20. Christ, T., Wettwer, E., Dobrev, D., Adolph, E., Knaut, M., Wallukat, G., and Ravens, U. Autoantibodies against the beta(1)-adrenoceptor from patients with dilated cardiomyopathy prolong action potential duration and enhance contractility in isolated cardiomyocytes. J Mol Cell Cardiol **33,** 1515, 2001.
21. Neidlinger-Wilke, C., Grood, E., Claes, L., and Brand, R. Fibroblast orientation to stretch begins within three hours. J Orthop Res **20,** 953, 2002.
22. Berry, J.L., Steen, J.A., Williams, J.K., Jordan, J.E., Atala, A., and Yoo, J.J. Bioreactors for development of tissue engineered heart valves. Ann Biomed Eng **38,** 3272, 2010.
23. Gandaglia, A., Bagno, A., Naso, F., Spina, M., and Gerosa, G. Cells, scaffolds and bioreactors for tissue-engineered heart valves: a journey from basic concepts to contemporary developmental innovations. Eur J Cardiothorac Surg **39,** 523, 2011.
24. Colombo, A., Cahill, P.A., and Lally, C. An analysis of the strain field in biaxial Flexcell membranes for different waveforms and frequencies. Proc Inst Mech Eng H **222,** 1235, 2008.
25. Boerboom, R.A., Rubbens, M.P., Driessen, N.J.B., Bouten, C.V.C., and Baaijens, F.P.T. Effect of strain magnitude on the tissue properties of engineered cardiovascular constructs. Ann Biomed Eng **36,** 244, 2008.
26. Tulloch, N.L., Muskheli, V., Razumova, M.V., Korte, F.S., Regnier, M., Hauch, K.D., Pabon, L., Reinecke, H., and Murry, C.E. Growth of engineered human myocardium with mechanical loading and vascular coculture. Circ Res **109,** 47, 2011.
27. Caspi, O., Lesman, A., Basevitch, Y., Gepstein, A., Arbel, G., Huber, I., Habib, M., Gepstein, L., and Levenberg, S. Tissue engineering of vascularized cardiac muscle from human embryonic stem cells. Circ Res **100,** 263, 2007.
28. Radisic, M., Park, H., Martens, T.P., Salazar-Lazaro, J.E., Geng, W.L., Wang, Y.D., Langer, R., Freed, L.E., and Vunjak-Novakovic, G. Pre-treatment of synthetic elastomeric scaffolds by cardiac fibroblasts improves engineered heart tissue. J Biomed Mater Res A **86A,** 713, 2008.
29. Yang, G.G., Crawford, R.C., and Wang, J.H.C. Proliferation and collagen production of human patellar tendon fibroblasts in response to cyclic uniaxial stretching in serum-free conditions. J Biomech **37,** 1543, 2004.
30. Wang, J.H.C., and Grood, E.S. The strain magnitude and contact guidance determine orientation response of fibroblasts to cyclic substrate strains. Connect Tissue Res **41,** 29, 2000.
31. Wang, J.H.C. Substrate deformation determines actin cytoskeleton reorganization: a mathematical modeling and experimental study. J Theor Biol **202,** 33, 2000.
32. Wang, J.H.C., Goldschmidt-Clermont, P., Wille, J., and Yin, F.C.P. Specificity of endothelial cell reorientation in response to cyclic mechanical stretching. J Biomech **34,** 1563, 2001.
33. Zhou, J.W., Ellis, A.V., and Voelcker, N.H. Recent developments in PDMS surface modification for microfluidic devices. Electrophoresis **31,** 2, 2010.
34. Bokenes, J., Sjaastad, I., and Sejersted, O.M. Artifactual contractions triggered by field stimulation of cardiomyocytes. J Appl Physiol **98,** 1712, 2005.
35. Zimmermann, W.H., Schneiderbanger, K., Schubert, P., Didie, M., Munzel, F., Heubach, J.F., Kostin, S., Neuhuber, W.L., and Eschenhagen, T. Tissue engineering of a differentiated cardiac muscle construct. Circ Res **90,** 223, 2002.

Address correspondence to:
Ursula Ravens, MD, PhD
Department of Pharmacology and Toxicology
Medical Faculty "Carl Gustav Carus"
Dresden University of Technology
Fetscherstr. 74
Dresden D-01307
Germany

E-mail: ravens@mail.zih.tu-dresden.de

Received: March 1, 2012
Accepted: September 6, 2012
Online Publication Date: December 10, 2012